This is an Accepted Manuscript of an article published by Taylor & Francis in Combustion science and technology on 25 Feb 2022 (Published online), available online: http://www.tandfonline.com/10.1080/00102202.2022.2041000.

Limits of Sustaining a Flame above Smoldering Woody Biomass

Yuying Chen[1], Zhirong Liang[1], Shaorun Lin[1,2,*] and Xinyan Huang[1,*]

[1]*Research Centre for Fire Safety Engineering, The Hong Kong Polytechnic University, Hong Kong*

[2]*Hong Kong Polytechnic University Shenzhen Research Institute, Shenzhen, Guangdong, China*

**Corresponding to flynn.lin@connect.polyu.hk* (SL); *xy.huang@polyu.edu.hk* (XH)

Abstract: Smoldering is slow, low-temperature, and flameless burning of porous fuel, and it is also an emerging method for energy conversion and waste removal. However, smoldering combustion is an incomplete combustion process, so the pollutions from the smoldering emissions are significant concerns. This work explores the flaming of emission gases from the smoldering wood chips (200 kg/m^3) under different oxidizer flow velocities (4 mm/s-24 mm/s) and oxygen concentrations (14%-21%) through porous media. Once ignited on the top, the smoldering front first propagates downward (1st stage, opposed) to the bottom and then propagates upward (2nd stage, forward). We found that during the 1st-stage downward smoldering propagation, a stable flame of smoldering emissions could be piloted and sustained. The critical smoldering burning rate for maintaining a stable flame remains constant at 10-12 g/m^2·s. To reach such a minimum smoldering burning rate, the required opposed flow velocity increases from 6 to 24 mm/s, as the oxygen concentration decreases from 21 to 14%. A simplified heat transfer process is proposed to reveal the limiting conditions for the co-existence of flaming and smoldering. This work enriches strategies for the clean treatment of smoldering emissions and promotes an energy-efficient and environment-friendly method for biowaste removal.

Keywords: *Smoldering combustion; Flammability limit; Fire spread; Porous media; Oxygen concentration*

Nomenclature

Symbols		***Greeks***	
C	constant (mm/s)	v	stochiometric coefficient (-)
D	diameter (m)	ρ	density (kg/m^3)
h	convection coefficient (W/(m^2-K))		
ΔH	heat of reaction (MJ/kg)	***Subscripts***	
k	thermal conductivity (W/(m-K))	∞	ambient
$\dot{m}''$	mass flux (g/m^2·s)	c	cooling
$\dot{q}''$	heat flow (kW/m^2)	crt	critical
S	spread rate (m/s)	f	flame
t	time (s)	F	fuel
u	flow velocity (m/s)	g	gas
T	temperature (°C/K)	py	pyrolysis
X	volume fraction (%)	sm	smoldering
Y	mass fraction (%)	w	wall

1. Introduction

Smoldering is slow, low-temperature, and flameless burning of porous fuels and one of the most persistent types of combustion phenomena (Ohlemiller 1985; Rein 2014; Torero *et al.* 2020). Smoldering is a heterogeneous process sustained when oxygen directly attacks the hot fuel surface, which is the dominant burning phenomenon of reactive porous media like woods (Jones *et al.* 1968; Anca-Couce *et al.* 2012), coals (Melody and Johnston 2015), and organic soils (Huang and Rein 2016; Lin *et al.* 2020). Generally, the combustion of the porous media can be approximated as two lumped chemical pathways, namely, pyrolysis and oxidation (Rein 2013; Lin *et al.* 2019). Pyrolysis will result in pyrolysis gas and char, which are both susceptible to subsequent oxidative reactions (Rein 2014). The oxidation of char leads to smoldering combustion, while the gas-phase oxidation leads to flaming combustion (Rein 2009).

Although there are some similarities between flaming and smoldering combustion (Lin and Huang 2021), smoldering is fundamentally different from flaming in terms of reaction chemistry and transport processes (Palmer 1957; Ohlemiller 1985; Rein 2014). The initiation of smoldering requires a relatively small amount of energy (Lin *et al.* 2019), and it may be sustained at an oxygen concentration as low as 12% and a moisture content higher than 100% (Huang and Rein 2016; Huang *et al.* 2016). In general, the maximum smoldering temperature ranges from 500 to 800 ℃, depending on the fuel types and operation conditions (Rein 2014), which is much lower than the flame temperature (>1100 ℃) (Law 2010). However, with a rich oxygen supply, the maximum smoldering temperature may exceed 1000 °C (Gao *et al.* 2021; Huang and Gao 2021), causing the smoldering-to-flaming (StF) transition (Santoso *et al.* 2019) or the co-existence of smoldering and flaming (Huang and Gao 2021; Lin, Huang, *et al.* 2021).

Flaming combustion is one of the most effective ways to fast remove municipal solid wastes (MSW). Incineration as a conventional waste combustion method has been used worldwide (Shin *et al.* 2000; Tarelho *et al.* 2011; Barnes 2015), and cofiring wastes with primary fuel (e.g. coal and natural gas) (Tillman 2000; Dmitrienko *et al.* 2018) has been widely applied. Recently, smoldering combustion also has been proposed for organic waste removal and has been successfully demonstrated in the removal of bioliquids (Kinsman *et al.* 2017; Zanoni *et al.* 2019), feces (Fabris *et al.* 2017; Yermán *et al.* 2017), sludges (Rashwan *et al.* 2016), oil shales (Martins *et al.* 2010), and food wastes (Song *et al.* 2022). Smoldering reactor has a lower combustion temperature (500-800 ℃), which improves the safety of the waste removal process. Smoldering waste removal can also minimize the pre-treatment processes and handle different kinds of organic wastes with high moisture contents (Yermán *et al.* 2015; Rashwan *et al.* 2016). Smoldering-based technology has a great potential to improve the process efficiency by controlling oxygen supply (Vantelon *et al.* 2005; Pironi *et al.* 2009; Yerman *et al.* 2017).

On the other hand, as an incomplete combustion process, smoldering generates many pollutions, posing severe threats to humans and the environment (Hu *et al.* 2018). The primary smoldering emissions include greenhouse gases (CO_2, CH_4), toxic compounds (e.g., CO, volatile organic carbon (VOC), NH_3), and particulate matters (PMs) (Michel *et al.* 2005; Van Der Werf *et al.* 2006; Wiedinmyer

et al. 2006). Specifically, smoldering combustion has higher emission factors (EFs) of incomplete combustion products, such as CO and CH_4 than flaming combustion. And PM derived from smoldering combustion varies greatly from PM_1 to PM_{10} (Iinuma *et al.* 2007; Tissari *et al.* 2008). However, most smoldering emissions are still flammable because they still contain a large number hydrocarbon pyrolysis gases and CO (Wang *et al.* 2021). In contrast, a flame can convert most smoldering emission gases into H_2O and CO_2 (Rein 2014). By sustaining a flame above the smoldering process not only can generate extra heat, but also remove a large portion of flammable and toxic smoldering emissions, thus, promoting more efficient and cleaner smoldering applications. However, the co-existence of flaming and smoldering on biomass has not been well explored so far, posing a knowledge gap.

The purpose of this study is to explore whether the emissions from smoldering wood can sustain a robust flame. Considering the oxygen supply is a key parameter of smoldering combustion, the critical airflow velocities (4-24 mm/s) and oxygen concentrations (14-21%) for the co-existence of smoldering and flaming are quantified experimentally and analyzed theoretically. The results are expected to help promote more environment-friendly and energy-efficient smoldering applications.

2. Experimental method

2.1 Setup and fuel preparation

Wood chips, as representative biomass fuel and typical biowaste, were chosen in this experiment (Fig. 1). The particle size of the wood chips ranges from 2 mm to 20 mm, with an average of 12 mm, provided by a local wood recycling company (ECO-Greentech Ltd.). The dry bulk density, solid density, and porosity were measured to be 200 ± 10 kg/m^3, 600 ± 20 kg/m^3, and 0.67, respectively. Before the test, the raw wood chips were thoroughly dried in an oven at 90 ℃ for 48 h and then stored in a sealed box to avoid the re-absorption of the ambient moisture (about 5% on the mass basis). The thermal analysis for the wood samples was conducted with a PerkinElmer STA 6000 Simultaneous Thermal Analyzer in both air and nitrogen atmospheres, and the representative data are shown in Appendix (Fig. A1).

The schematic diagram of the experimental setup is also shown in Fig. 1, and it mainly consisted of a tubular smoldering reactor, an ignition system, an oxidizer supply system, and two video cameras. The top-open smoldering reactor was made of 3-mm thick stainless steel, and it had a depth of 27 cm and an internal diameter of 13 cm. A 1-cm ceramic insulation layer was attached to the surface of the reactor to reduce the heat losses. Initially, a 5-cm sand layer was poured into the bottom of the reactor. Afterward, a test sample with a controlled mass of 405 ± 5 g was placed above the sand layer with a constant height of 15 cm. To monitor the smoldering temperature, an array of eight K-type thermocouples (1-mm bead diameter) was inserted from the sidewall into the fuel sample, and their beads were aligned along the reactor axis from 0 cm (bottom) to 14 cm (1 cm below the top surface) with an interval of 2 cm. To better observe the location and intensity of the glowing smoldering front, the glass tubular reactor was also used during the tests and was monitored by a side-view camera.

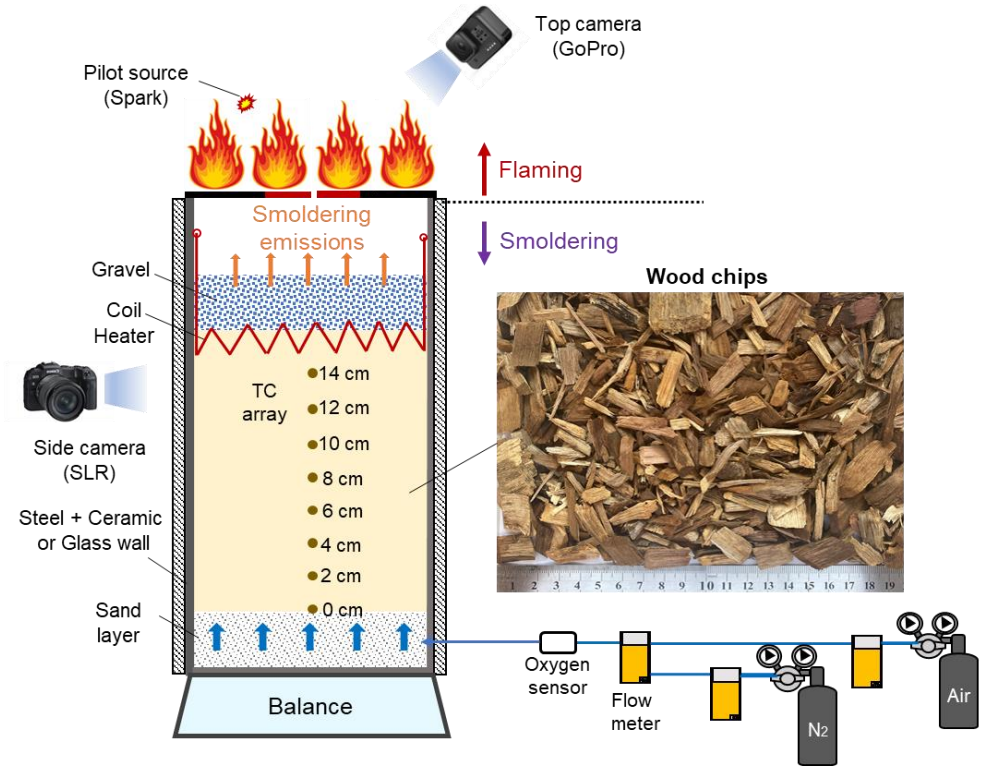

Fig. 1. Schematic diagram of the experimental setup and the photo of wood chips samples.

A coil heater buried 1 cm below the surface of wood chips was used to initiate the smoldering combustion, and a lighter or a spark (as a pilot source) was installed at 2 cm above the outlet of the reactor. A forced oxidizer flow was supplied from the bottom of the reactor, and the flow rate was controlled by the flow meter. The oxygen concentration of the input oxidizer was modified by adding N_2 to the air stream. The experiments control two parameters for the smoldering reactor:

(1) the bulk internal flow velocities (u_g) from 4 mm/s to 24 mm/s, that is, the mass flowrate ($\dot{m}_g'' = \rho_g u_g$) from 4.8 g/m^2-s to 28.8 g/m^2-s, and

(2) the inflow oxygen concentrations, denoted by the volume fraction (X_{O_2}) from 14% to 21%.

Together, the overall oxygen inflow rates ($\dot{m}_{O_2}'' = \rho_g Y_{O2} u_g$) changes from 1.1 g/m^2-s to 6.6 g/m^2-s (see Table 1). Note that the flow velocity was an overall value for the porosity of 1, and for the current wood-chip bed with a porosity of 0.67, the average velocity through the pores was 4.5 mm/s to 36 mm/s. The oxidizer flow was homogenized by the 5-cm sand layer below the wood chips. A top-view GoPro camera was used to record the experiment.

2.2 Experimental procedure

The smoldering combustion was initiated by the coil heater with the ignition protocol at 100 W for 15 min, which was strong enough to generate a robust smoldering for the dry wood chips. After ignition, a layer of fine and clean gravel with a height of 7 cm was placed on the fuel surface, as shown in Fig. 1. This fine gravel layer prevented (1) the flying ash, (2) flame from flashing back to the smoldering

reactor, and (3) the internal smoldering-to-flaming transition under a large high airflow rate, and it also provided an insulation layer to prevent the flame from directly heating the solid fuel.

Afterwards, the forced oxidizer flow was then fed from the bottom with a prescribed flow velocity and oxygen concentration. Afterward, a lighter or a spark near the outlet was applied to ignite the emissions released from the smoldering fuel. If the flame was successfully piloted and self-sustained, the oxidizer flow velocity and oxygen concentration were gradually adjusted to find the limiting conditions. The experiments were stopped when all thermocouple measurements were below 200 ℃. For each case, at least three repeating tests were carried out to ensure the repeatability of the experiments. During the tests, the ambient temperature (T_a) was 23 ± 2 ℃, and the relative humidity was 50 ± 10%, and the pressure was 1 atm.

3. Results and discussion

3.1 Co-existence of smoldering and flaming

To show the smoldering process clearly, photos of smoldering in the glass tubular reactor are presented. Fig. 2 (a) shows an example of fire phenomena at a relatively low internal airflow velocity of 4 mm/s, where the smoldering combustion was observed, but no flame was successfully piloted (see Video S1 in *Supplemental materials*). Once the electrical heating was applied, a reaction front was observed near the top surface, which was hot enough to emit visible light (glowing incandescence) (Huang and Gao 2021). After ignition, there were two smoldering propagation stages, namely 1st-stage downward propagation and the 2nd-stage upward propagation, which were the same as past findings (Huang and Rein 2017, 2019; Lin and Huang 2021; Wang *et al.* 2021).

In the 1st-stage downward propagation, the smoldering front moved as opposed to the internal airflow, and its structure included a drying sub-front, a fuel-pyrolysis sub-front, and a char oxidation sub-front. The endothermic pyrolysis of wood generated the gaseous pyrolysates and solid char as

$$\text{Wood} \xrightarrow[\text{smoldering}]{\text{heat}} \nu_{py}\text{Pyrolysates} + \left(1-\nu_{py}\right)\text{Char} \qquad \text{(Wood pyrolysis)} \quad (1)$$

Thus, the white smoke was always observed, which was in the form of condensed tiny droplets of the pyrolysis gases and water vapor (Lin and Huang 2021). The pyrolysis front was driven by the exothermic char oxidation

$$\text{Char} + \text{O}_2 \rightarrow \text{Ash} + \text{CO}_2 + \text{H}_2\text{O (g)} + \text{other gases} + \text{Heat} \qquad \text{(Char oxidation)} \quad (2)$$

Note that not all chars were oxidized or burnt because only a limited oxygen supply was provided from the bottom. This heterogeneous char oxidation produced a mixture of hydrocarbons, CO_2, and CO (Rein *et al.* 2009; Lin, Huang, *et al.* 2021). Nevertheless, the smoldering emission gases (from both wood-pyrolysis and char-oxidation) cannot be piloted to sustain a flame, because under such a low airflow supply, the pyrolysis process inside the smoldering front was too weak to release sufficient fuel gases.

As the smoldering front approached the fuel-bed bottom, it transitioned to the 2nd-stage upward propagation mode to burn out all the remaining char. Then, the internal airflow was in the same direction as the smoldering propagation (i.e., the forward smoldering). For forward smoldering, it is essentially a fuel-regression process, where the smoldering front moved due to the burnout of fuel (Huang and Rein 2019; Huang and Gao 2021; Lin and Huang 2021). The fuel for the 2nd stage propagation was primary char, so the char oxidation dominated, where more black smoke was observed. Eventually, wood chips were almost burned out and turned into white ash accompanied by a small amount of char. During the whole process, no flame could be piloted.

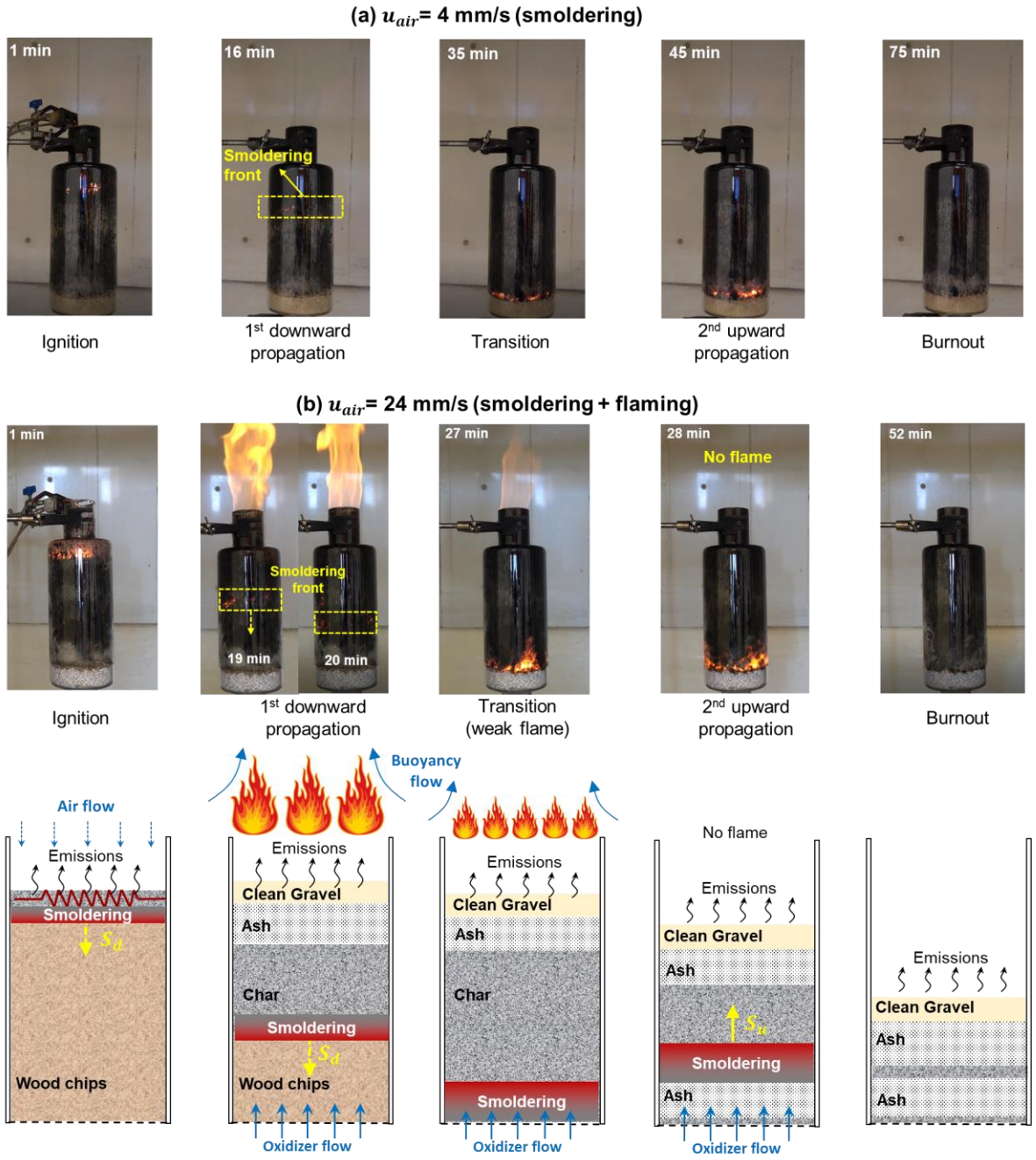

Fig. 2. Snapshots of combustion phenomena of wood chips under airflow velocity of (a) 4 mm/s and (b) 24 mm/s with schematic diagrams (also see Videos S1 and S2).

Fig. 2(b) displays the burning process (photos and schematic diagram) at a higher airflow velocity of 24 mm/s (see Video S2). Compared to the low-flow case in Fig. 2(a), a similar two-stage smoldering propagation was observed, while the glowing smoldering front was brighter. More importantly, a flame could be piloted and sustained outside the reactor, co-existing with the downward smoldering propagation. Therefore, we conclude that flame can co-exist with the intense smoldering biomass inside the reactor and burn out almost all smoldering emissions. The oxygen supply to the external flame mainly comes from the buoyant flow from the ambient rather than the internal flow, because the oxygen of internal flow has been consumed inside the smoldering front via char oxidation (Wang *et al.* 2021).

In the 1st-stage, the wood pyrolysis released large quantities of pyrolysates (e.g., CO, H_2, CH_4, C_2H_4, and C_2H_6) (Eq. 1) (Dufour *et al.* 2008), which were highly flammable (Quintiere 2006). The mass flux of these flammable pyrolysis gases was controlled by the strength of the smoldering (char-oxidation) front which could be intensified by oxygen supply. Once the abundant pyrolysis emissions were released, a flame could be piloted as

$$\text{Smoldering emissions} + O_2 \rightarrow CO_2 + H_2O\ (g) \qquad \text{(Flaming)} \quad (3)$$

The flame was initially intense with a bright orange color (see Fig. 2b) that consumed almost all smoldering emissions during the 1st stage and effectively mitigated the pollutants. Afterward, as the smoldering front gradually approached the fuel-bed bottom, the flame became weaker and shorter, and it eventually extinguished from the 2nd stage to the final burnout due to the end of pyrolysis.

3.2 Smoldering temperature

Fig. 3 shows the time evolution of the smoldering temperature at the airflow velocities of (a) 4 mm/s and (b) 24 mm/s of the same tests in Fig. 2(a-b). The trends of the temperature profiles at different airflow velocities are similar, which are characterized by two characteristic peak values.

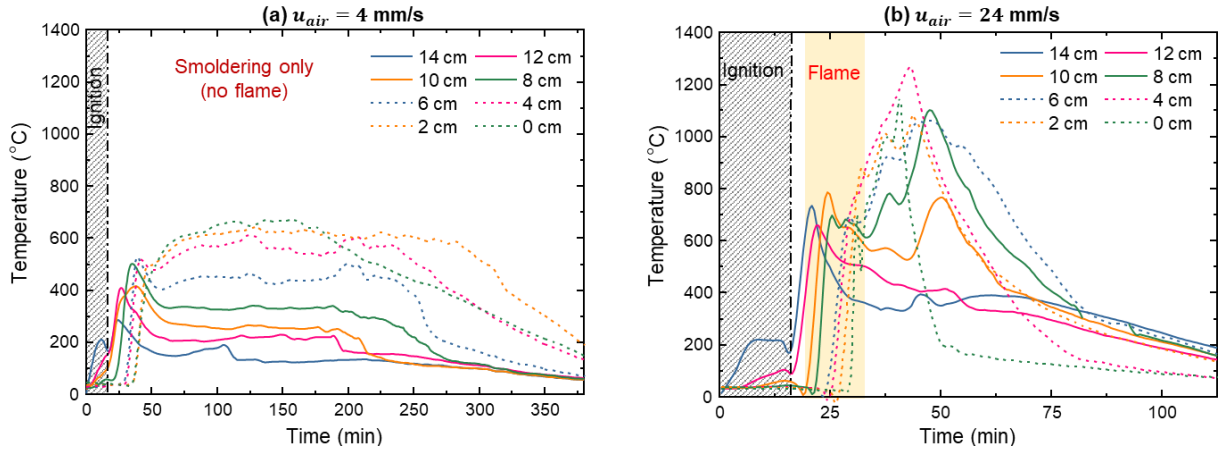

Fig. 3. Smoldering temperature profiles at the airflow velocity of (a) 4 mm/s and (b) 24 mm/s, where the orange-color shaded area indicates the co-existence of flaming and smoldering.

The (peak) smoldering temperature of the 1st stage ($T_{max,1}$) is usually lower than that of the 2nd stage ($T_{max,2}$), consistent with the findings from previous studies (Huang and Rein 2017; Wang *et al.* 2017; Lin and Huang 2021). It is because (1) the biomass pyrolysis is endothermic, and (2) additional heat is required to maintain a fast propagation front in the 1st stage (Huang and Rein 2017, 2019). Afterward, as the pyrolysis front reaches the bottom, only char oxidation exists, and the reaction front stays on the bottom, so a higher temperature is observed.

Fig. 4a and Table 1 further summarize the average values of the peak temperature of two stages ($T_{max,1}$ and $T_{max,2}$) under varying airflow velocity (21% oxygen). As expected, both peak temperatures increase with the airflow velocity, because of stronger char oxidation. For example, as the airflow velocity increases from 4 to 24 mm/s, the 1st-stage peak ($T_{max,1}$) increases from 465 to 738 ℃, and the 2nd-stage peak ($T_{max,2}$) increases from 650 to 1294 ℃. However, as the flow velocity continuously increases, their sensitivity to flow decreases, because the cooling effect of internal airflow becomes important (Lin, Chow, *et al.* 2021).

Table 1 Average values of peak temperature of 1st stage ($T_{max,1}$) and 2nd stage ($T_{max,2}$), duration of 1st stage (Δt_1) and 2nd stage (Δt_2), and maximum mass flux of wood smoldering ($\dot{m}''_{max}$) under different airflow velocities (u_{air}) with X_{O_2} =21% , gas inflow rates ($\dot{m}''_g = \rho_g u_g$), and oxygen flow rates ($\dot{m}''_{O_2} = \rho_g Y_{O2} u_g$).

u_{air} (mm/s)	$\dot{m}''_g$ (g/m²·s)	$\dot{m}''_{O_2}$ (g/m²·s)	$T_{max,1}$ (℃)	Δt_1 (min)	$T_{max,2}$ (℃)	Δt_2 (min)	$\dot{m}''_{max}$ (g/m²·s)
4	4.8	1.1	465 ± 33	54 ± 3	650 ± 20	386 ± 10	5.3 ± 0.5
5	6.0	1.4	473 ± 45	44 ± 4	700 ± 22	320 ± 9	8.0 ± 0.6
7	8.4	1.9	493 ± 23	37 ± 4	788 ± 36	217 ± 10	10.3 ± 0.4
9	10.8	2.5	514 ± 43	31 ± 2	927 ± 29	178 ± 8	15.0 ± 0.6
12	14.4	3.3	619 ± 48	26 ± 3	1140 ± 29	113 ± 7	16.8 ± 0.5
18	21.6	4.9	678 ± 30	18 ± 2	1180 ± 32	76 ± 8	21.4 ± 0.4
24	28.8	6.6	738 ± 35	15 ± 2	1294 ± 26	71 ± 5	22.7 ± 0.7

Table 2 Average values of peak temperature of 1st stage ($T_{max,1}$) and 2nd stage ($T_{max,2}$), and duration of 1st stage (Δt_1) and 2nd stage (Δt_2) under different oxygen concentrations (X_{O_2}) when the bulk internal flow velocity is $u_g = 12$ mm/s. The gas inflow rate is $\dot{m}''_g = \rho_g u_g$, and the oxygen flow rate is $\dot{m}''_{O_2} = \rho_g Y_{O2} u_g$.

X_{O_2} (%)	$\dot{m}''_g$ (g/m²·s)	$\dot{m}''_{O_2}$ (g/m²·s)	$T_{max,1}$ (℃)	Δt_1 (min)	$T_{max,2}$ (℃)	Δt_2 (min)
14	13.5	2.2	581 ± 44	50 ± 4	836 ± 24	184 ± 7
15	13.6	2.3	588+48	46 ± 3	841 ± 30	157 ± 5
16	13.6	2.5	597 ± 31	40 ± 4	930 ± 26	149 ± 6
18	13.7	2.8	610 ± 47	31 ± 5	1015 ± 20	140 ± 10
21	14.4	3.3	619 ± 48	26 ± 3	1140 ± 29	113 ± 7

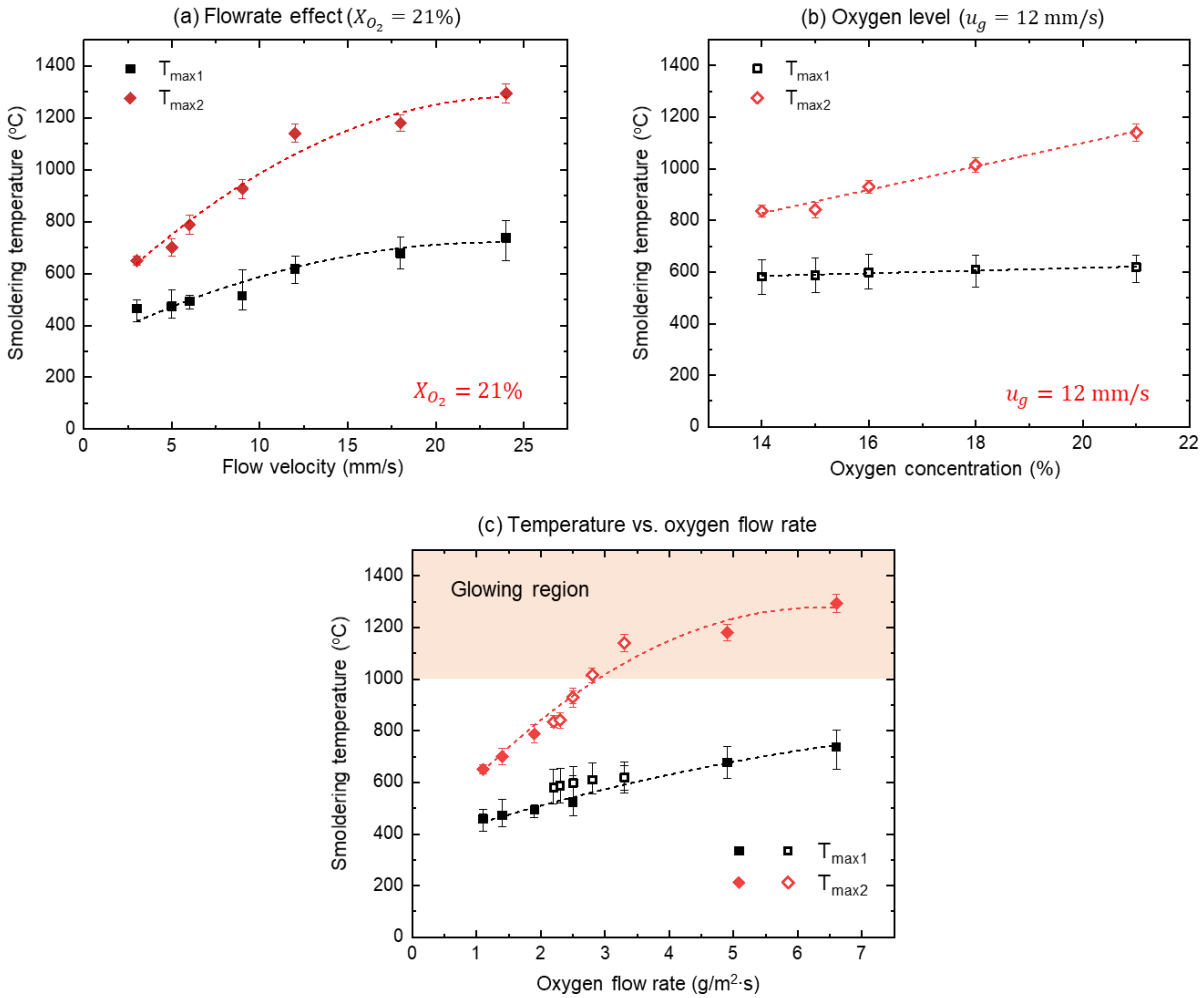

Fig. 4. Peak smoldering temperatures of two stages vs. (a) flow velocity, (b) oxygen concentration, and (c) oxygen flow rate where the error bars show the standard deviations of repeating tests.

Fig. 4b and Table 2 further summarize influence of inflow oxygen concentration on the average values of the peak temperature of two stages ($T_{max,1}$ and $T_{max,2}$) under a fixed bulk internal flow velocity of $u_g = 12$ mm/s. As the oxygen concentration increases, 2nd-stage peak temperature ($T_{max,2}$) increases clearly because of stronger char oxidation. Nevertheless, the first stage peak temperature ($T_{max,1}$) is insensitive to the oxygen concentration. It is probably because the first stage is a heat-transfer controlled smoldering process, and not consuming all the oxygen flow (Wang *et al.* 2021). Then, the smoldering temperature shows a more significant increase with the flow velocity than the oxygen concentration, mainly because a wider range of oxygen flow rate is supplied by changing the flow velocity from 4-24 mm/s, as shown in Fig. 4c.

3.3 Critical fuel-burning mass flux

The burning mass flux ($\dot{m}''$) is the mass loss rate per unit area of the fuel, which is an important parameter to quantify the combustion limits (Rich *et al.* 2007). Fig. 5 shows the time evolution of the remaining mass fraction and the mass flux of the burning of wood under two representative internal

airflow rates of (a) 4 mm/s and (b) 18 mm/s. Within a shorter period, nearly 60% of the fuel mass is consumed in the 1st-stage downward smoldering due to the release of all pyrolysates. This is also supported by TGA results under inert atmosphere (Fig. A1a), where 50-70% wood mass is lost due to pyrolysis depending on the final temperature. Although the 2nd char-oxidation smoldering stage lasts for a much longer period, the mass loss is smaller than 40%, and the burning mass flux remains stable at about 1-2 g/m^2·s until burnout.

At the low airflow velocity of 4 mm/s (Fig. 5a), the maximum mass flux is about 4.3 g/m^2·s in the 1st-stage, and the flame of smoldering emission cannot be piloted. As the internal airflow velocity is increased to 18 mm/s, the maximum mass flux is increased to 22 g/m^2·s. As a result, a flame can be piloted outside when the smoldering burning flux reaches about 10 g/m^2·s, co-existing with smoldering (Fig. 5b). The solid symbol in Fig. 5b represents the moment of flame ignition, and the hollow symbol signifies the moment of flame extinction. The critical mass flux for flame ignition is similar to that of flame extinction at about 11 ± 1 g/m^2·s.

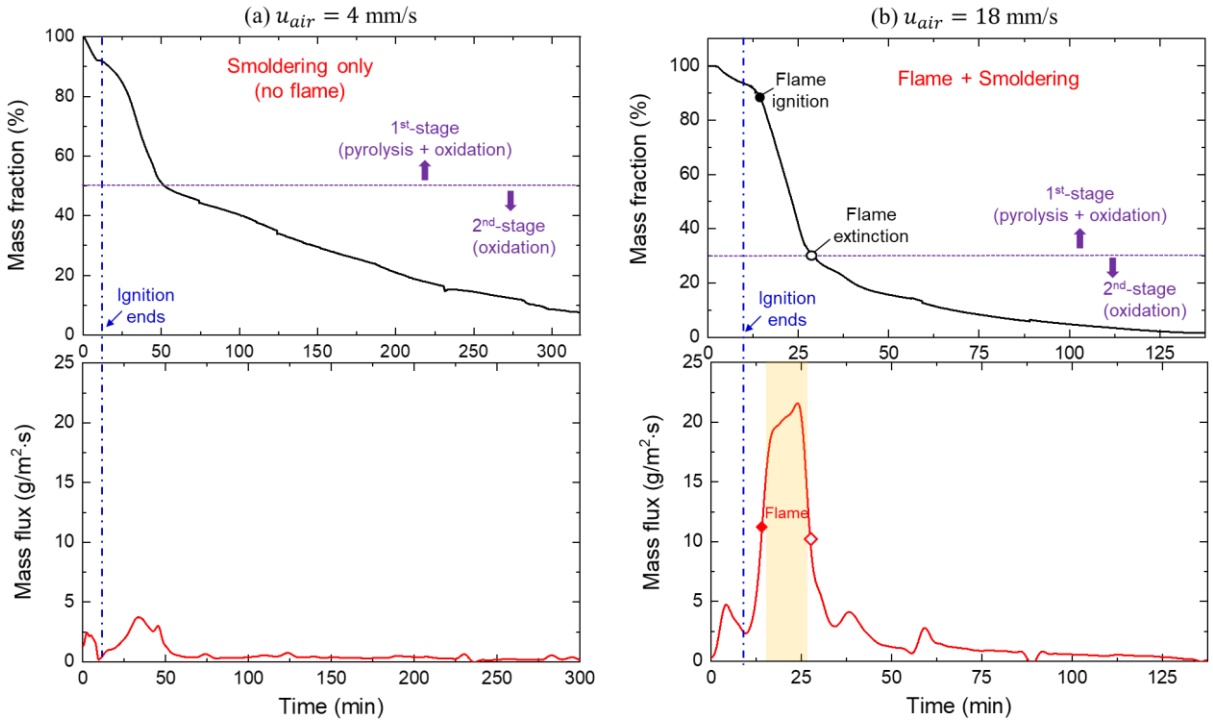

Fig. 5. Evolution of fuel mass fraction and mass flux under the internal airflow velocity of (a) 4 mm/s and (b) 18 mm/s, where the oxygen concentration is 21%.

Fig. 6 further summarizes the maximum fuel smoldering mass flux under different airflow velocities, as well as the critical mass flux for the co-existence of flaming and smoldering. As shown in Fig.6, the maximum mass flux increases from 5.3 g/m^2·s to 22.7 g/m^2·s, as the airflow velocity increases from 4 mm/s to 24 mm/s. However, the critical mass flux for piloting a flame on the wood-chip smoldering emissions or the co-existence of flaming and smoldering is almost constant at 11 ± 1 g/m^2·s. Moreover, as the airflow velocity is lower than about 6 mm/s, the maximum mass flux is below such a critical mass

flux required for flame ignition. Therefore, we can also define a minimum airflow velocity for the 1st-stage smoldering front to sustain the flame on the smoldering emission, that is, 6 mm/s with 21% oxygen concentration.

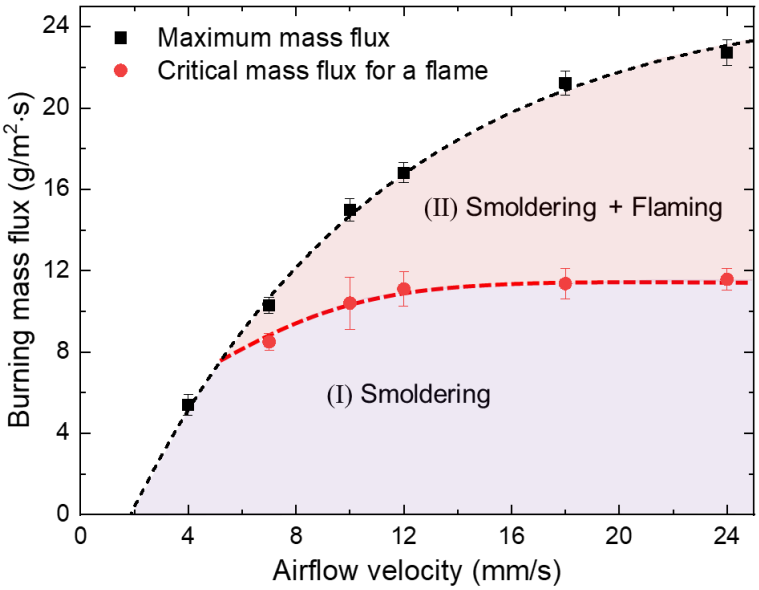

Fig. 6. The maximum mass flux of smoldering burning and the critical mass flux for the co-existence of flaming and smoldering vs. the airflow velocity. The error bars of the maximum mass flux represent the standard deviations of repeating tests, the error bars of critical mass flux represent the points for flame ignition (average upper boundary) and flame extinction (average lower boundary), and the lines are the manual fitting curves.

3.4 Flame duration

Fig. 7 shows the durations of two smoldering stages versus airflow velocities from 4 mm/s to 24 mm/s. The duration of co-existed flame is also compared, where the flame must be stable, and the smoke from smoldering is almost consumed by the flame. In general, the durations for all combustion processes decrease, as the airflow velocity increases. The rising oxygen supply and oxidation rate increase the smoldering temperature, thus, accelerating both the heat-transfer and burning processes (Lin, Huang, *et al.* 2021). The 1st-stage downward smoldering lasts for a much shorter period than the 2nd-stage upward propagation. For instance, at the airflow velocity of 7 mm/s, the duration of the 2nd smoldering stage (217 min) is about sixfold of the 1st stage (37 min).

For the duration of flame, it is slightly shorter than that of the 1st smoldering stage, because the flame can only be piloted after reaching the critical smoldering mass flux of 11 ± 1 g/m^2·s. Thus, the flaming duration follows the same trend of 1st-stage smoldering, which decreases with the increase of airflow velocity. Specifically, at the airflow velocity of 7 mm/s, the flame duration is 25 min, which is 12 min less than the duration of 1st-stage smoldering. As the airflow velocity increases to 24 mm/s, the flame duration is the same as the 1st-stage smoldering, because of an intensive smoldering front.

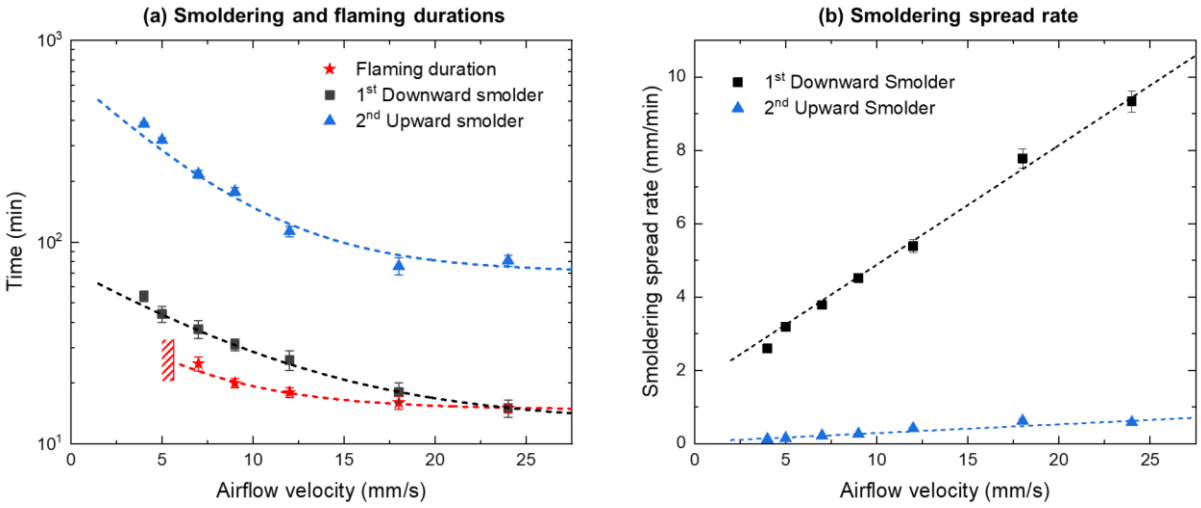

Fig. 7. Duration of the flame and smoldering propagation at different airflow velocities, where symbols show the experimental data (with standard deviations), and lines are the manual fitting curves.

3.5 Effect of oxygen concentration

The effect of the oxygen concentration on the critical (minimum) flow velocity (u_{crt}) for the co-existence of smoldering and flaming is shown in Fig. 8. The critical oxidizer flow velocity increases significantly as the oxygen concentration decreases. As previously shown in Fig. 6, the critical flow velocity of air (X_{O_2} =21%) required for maintaining a flame is 6 mm/s. As the oxygen concentration (X_{O_2}) decreases to 18%, 16%, 15%, and 14%, the critical oxidizer velocity increases to 8 mm/s, 11 mm/s, 18 mm/s, and 24 mm/s, respectively. By fitting the experimental data in Fig. 8, we can find an empirical correlation for the critical flow velocity (u_{crt}) and oxygen concentration (X_{O_2}) for the co-existence of smoldering and flaming as

$$u_{crt} = \frac{0.53}{Y_{O_2} - 11.6\%} \tag{4}$$

where the R^2 value is 0.96, showing a good quality of fitting.

The effect of oxygen concentration on the smoldering temperature is also shown in Fig. 3(b). The peak temperature of the 2nd smoldering stage (T_{max2}) increases significantly with the oxygen concentration, whereas the 1st smoldering stage temperature (T_{max1}) is not so insensitive to the oxygen concentration. This is because the oxygen has a relatively weak effect on the wood pyrolysis in the 1st stage, while the 2nd-stage smoldering temperature is dominated by char oxidation. Moreover, increasing either the oxygen concentration or flow rate can lead to a stronger and taller flame because (1) the pyrolysis process inside the smoldering front becomes stronger (i.e., more gaseous fuels emitted), and (2) the flame becomes partial premixed with the internal flow (i.e., some oxygen is not fully consumed in the smoldering front).

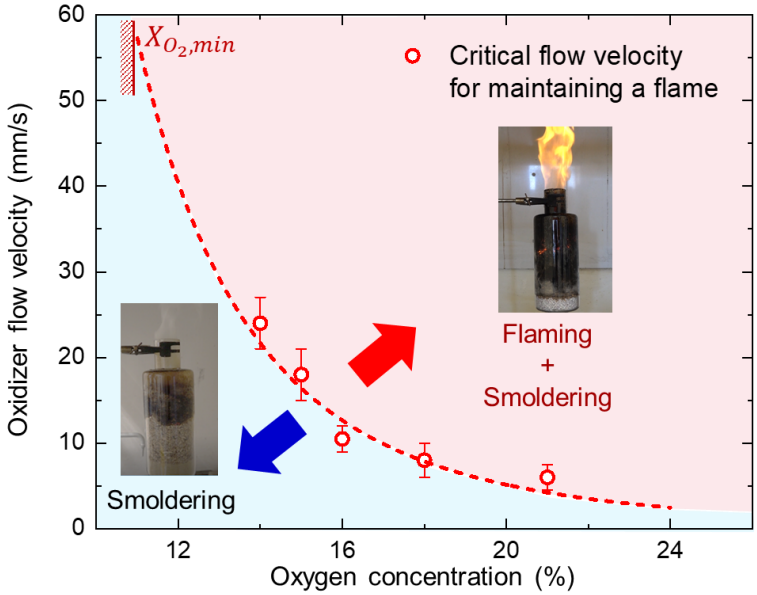

Fig. 8. Critical oxidizer flow velocity (u_{crt}) for a stable flame under different oxygen concentrations (X_{O_2}) where the error bars represent the upper and lower boundaries of measuring points.

4. Theoretical analysis

4.1 Limits for flaming

In the conventional flaming process (e.g., a wood flame), the pyrolysis of wood is driven by the flame heat flux and other external heating, and the burning rate can be estimated by the mass transfer number (or B number) (Rich *et al.* 2007; Drysdale *et al.* 2011). In this work, the pyrolysis of wood chips is driven by the exothermic char oxidation inside the smoldering front, making a fundamental difference. To further understand the co-existence of flaming and smoldering combustion on wood and other biomass, the limiting conditions for both (1) igniting and maintaining a flame and (2) the required smoldering front should be quantified.

To ignite and maintain a flame, a minimum mass flux of fuel gas is required. In the fire research community, such limiting conditions are called the "flash point" (to pilot a flame) and "fire point" (to maintain a piloted flame) (Rich *et al.* 2007; Drysdale *et al.* 2011). The limiting conditions of a robust and stable flame are considered in this research, so it is essentially a "fire point" rather than a flashpoint. A simplified heat transfer analysis is proposed for the premixed fuel gases and flame, as illustrated in Fig. 9(a).

The flame heat release rate ($\dot{q}''_f$) by burning the premixed pyrolysis gas should at least overcome the heat loss to the environment ($\dot{q}''_\infty$) and burner wall ($\dot{q}''_w$) as

$$\dot{q}''_f = \dot{m}''_{py,crt}\Delta H_f = \dot{q}''_\infty + \dot{q}''_w \quad (5)$$

where $\dot{m}''_{py,crt}$ is the minimum mass flux of pyrolysis gases; and ΔH_f is the heat of flaming combustion. Therefore, a minimum amount of pyrolysis gases should be generated to maintain the flame right above the fuel, which is found to range from 2 to 10 g/m^2·s for PMMA (Rich *et al.* 2007), wood (Emberley *et*

al. 2017), and peat (Lin *et al.* 2019). In this research, the smoldering emission ($\dot{m}''_{sm}$) is also found to be a constant, but at a slightly higher value of 11 ± 1 g/m^2·s (see Section 3.3 and Fig. 6). It is because the total smoldering emissions also include the less flammable emission from char oxidation ($\dot{m}''_{sm} = \dot{m}''_{py} + \dot{m}''_{ox} > \dot{m}''_{py}$), although the pyrolysis gases of wood chips inside smoldering reactor is primary.

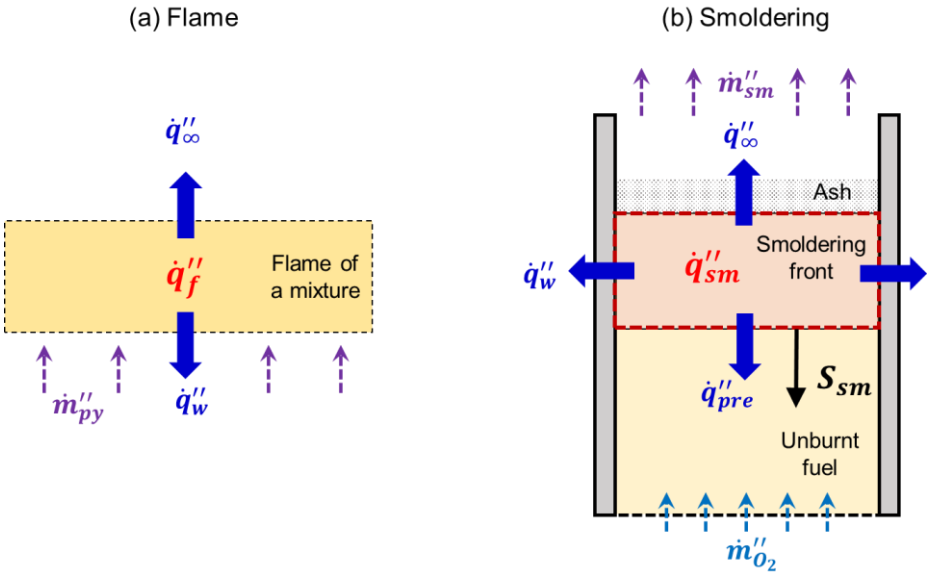

Fig. 9. The energy balance of (a) flame of a mixture and (b) smoldering front inside the reactor.

4.2 Limits for smoldering and oxygen supply

To generate a minimum mass flux of fuel gas for sustaining a flame, the smoldering front and char oxidation should be strong enough to drive a strong pyrolysis process. Therefore, the limiting condition of sustaining a flame becomes the limiting condition of the smoldering front. Then, a simplified heat transfer analysis is also proposed for the smoldering front, as illustrated in Fig. 9(b).

The smoldering heat release rate ($\dot{q}''_{sm}$) should first overcome the overall cooling rate ($\dot{q}''_{c}$) as

$$\dot{q}''_{sm} \geq \dot{q}''_{c} \tag{6}$$

In general, the smoldering front is cooled by the environment ($\dot{q}''_{\infty}$), reactor wall ($\dot{q}''_{w}$), and the preheat zone ($\dot{q}''_{pre}$). Moreover, it should also ensure strong pyrolysis to generate sufficient gaseous fuel ($\dot{m}''_{py,crt}$), which is controlled by the oxygen supply as

$$\dot{q}''_{sm} = \dot{m}''_{F}\Delta H_{sm} = \frac{\dot{m}''_{py,crt}}{\nu_{py}}\Delta H_{sm} = \dot{m}''_{O_2,crt}\Delta H_{ox} = \rho_g Y_{O_2} u_{crt}\Delta H_{ox} \tag{7a}$$

where ν_{py} is the stoichiometric coefficient of pyrolysis gas in Eq. (1); $\dot{m}''_{O_2,crt}$ is the critical mass flux of oxygen; ρ_g, Y_{O_2} and u_{crt} are the density, oxygen mass fraction, and critical velocity of the supplied oxidizer flow, respectively. By reorganizing, we have

$$u_{crt} = \frac{\dot{m}''_{py,crt}\Delta H_{sm}}{\nu_{py}\rho_g \Delta H_{ox} Y_{O_2}} \propto \frac{1}{Y_{O_2}} \tag{8a}$$

Therefore, the critical opposed flow velocity for the co-existence of flaming and smoldering combustion is inversely proportional to the oxygen concentration, which explains the overall trend of experimental data in Fig. 8.

As seen from Fig. 9 and Eq. (8), by decreasing the oxygen concentration, the required opposed flow velocity will dramatically increase to maintain an independent flame outside the smoldering reactor. However, as the flow velocity continuously increases, its direct cooling effect on the smoldering front can no longer be ignored. Eventually, smoldering will be blown off by a fast and oxygen-lean flow (Huang and Gao 2021; Lin, Chow, *et al.* 2021). The cooling of oxidizer flow could be considered as a reduction in the heat of oxidation as

$$\frac{\dot{m}''_{py,crt}}{\nu_{py}}\Delta H_{sm} = \dot{m}''_{O_2,crt}\Delta H_{ox} - \dot{q}''_{flow} \tag{7b}$$

where the cooling effect of internal flow is reflected by the increase of flow enthalpy after passing through the smoldering front as

$$\dot{q}''_{flow} = \nu_{em}\rho_g u_{crt} c_p (T_{sm} - T_\infty) \tag{9}$$

where ν_{em} is the stoichiometric coefficient of emission gases. Thus, there is minimum oxygen concentration ($Y_{O_2,min}$), below which the gas flow through the smoldering front become a net cooling ($\dot{m}''_{O_2,crt}\Delta H_{ox} - \dot{q}''_{flow} = 0$). From Eq. (7a), we can derive

$$Y_{O_2,min} = \frac{\nu_{em} c_p (T_{sm} - T_\infty)}{\Delta H_{ox}} \tag{10}$$

By re-arranging Eq. (7b), we have

$$u_{crt} = \frac{\dot{m}''_{py,crt}\Delta H_{sm}}{\rho_g \nu_{py}\Delta H_{ox}\left(Y_{O_2} - Y_{O_2,min}\right)} = \frac{C}{\left(Y_{O_2} - Y_{O_2,min}\right)} \tag{8b}$$

where $C = \dot{m}''_{py,crt}\Delta H_{sm}/\nu_{py}\rho_g\Delta H_{ox}$ is a fuel-related constant. Based on experimental data in Fig. 8 and Eq. (4), we can find that for the current fuel of wood chips, $C = 0.53$ [mm/s] and $Y_{O_2,min} \approx 11.6\%$.

On the other hand, if the forced oxygen supply is removed, there could still be a natural oxygen supply, driven by a minimum buoyancy and diffusion flow (u_{diff}) when the fuel is exposed to the ambient. In that case, there could also be an upper limit of the critical oxygen concentration, above which the co-existence of flaming and smoldering is guaranteed, even if under a very small natural diffusion flow. In the future, more experiments and numerical simulations can be conducted for different fuel types, flow compositions, and environmental conditions to explore the co-existence of flame and smoldering and further verify the limiting conditions.

5. Conclusions

In this work, we successfully verify that (1) the smoldering emission of wood chips can be piloted to sustain a flame and (2) flame can co-exist with smoldering combustion. With the smoldering ignition from the top and the flow from the bottom, the smoldering front first propagates downwards (1^{st}-stage opposed smoldering) to the fuel-bed bottom and then propagates upward (2^{nd}-stage forwards smoldering). The flame could only be piloted and self-sustained in the 1^{st}-stage smoldering because of an intense pyrolysis process within the smoldering front. The critical smoldering burning mass flux for maintaining a stable flame remains constant at 10-12 $g/m^2 \cdot s$.

The co-existence of flaming and smoldering depends on the oxygen supply to the smoldering front, which is verified by the theoretical analysis. The minimum opposed flow velocity required to maintain the stable flaming increases from 6 mm/s to 24 mm/s, as the oxygen concentration decreases from 21% to 14%. Moreover, increasing oxygen supply enhances the flame intensity and height, but the flame duration is reduced due to the accelerated burning processes. This work enriches strategies for the clean treatment of smoldering emissions and promotes an energy-efficient and environment-friendly method for biowaste removal. Future work will quantify the composition of smoldering emissions and determine the impacts of fuel types, moisture contents, and operational conditions on the co-existence of smoldering and flaming.

Declaration of Competing Interest

The authors declare that there is no conflict of interest.

Acknowledgements

This work is funded by National Natural Science Foundation of China (NSFC grant No. 51876183), ZJU SKLCEU Open Fund (2018012), Sichuan Science and Technology Program (2019YFSY0040), and Society of Fire Protection Engineers (SFPE) Educational & Scientific Foundation. Authors thanks ECO-Greentech Ltd. for providing fuel samples, and Prof. Jose Torero (University College London) for supporting the research idea and funding application.

References

Anca-Couce A, Zobel N, Berger A, Behrendt F (2012) Smouldering of pine wood: Kinetics and reaction heats. *Combustion and Flame* **159**, 1708–1719. doi:10.1016/j.combustflame.2011.11.015.

Barnes DI (2015) Understanding pulverised coal, biomass and waste combustion - A brief overview. *Applied Thermal Engineering* **74**, 89–95. doi:10.1016/j.applthermaleng.2014.01.057.

Dmitrienko MA, Legros JC, Strizhak PA (2018) Experimental evaluation of main emissions during coal processing waste combustion. *Environmental Pollution* **233**, 299–305. doi:10.1016/j.envpol.2017.10.090.

Drysdale D, Quintiere JG, Drysdale D (2011) 'An Introduction to Fire Dynamics.' (John Wiley & Sons, Ltd: Chichester, UK) doi:10.1002/9781119975465.

Dufour A, Celzard A, Fierro V, Martin E, Broust F, Zoulalian A (2008) Catalytic decomposition of methane over a wood char concurrently activated by a pyrolysis gas. *Applied Catalysis A: General* **346**, 164–173. doi:10.1016/j.apcata.2008.05.023.

Emberley R, Inghelbrecht A, Yu Z, Torero JL (2017) Self-extinction of timber. *Proceedings of the Combustion Institute* **36**, 3055–3062. doi:10.1016/j.proci.2016.07.077.

Fabris I, Cormier D, Gerhard JI, Bartczak T, Kortschot M, Torero JL, Cheng Y-L (2017) Continuous, self-sustaining smouldering destruction of simulated faeces. *Fuel* **190**, 58–66. doi:10.1016/j.fuel.2016.11.014.

Gao J, Qi X, Zhang D, Matsuoka T, Nakamura Y (2021) Propagation of glowing combustion front in a packed bed of activated carbon particles and the role of CO oxidation. *Proceedings of the Combustion Institute* **38**, 5023–5032. doi:10.1016/j.proci.2020.05.041.

Hu Y, Fernandez-Anez N, Smith TELL, Rein G (2018) Review of emissions from smouldering peat fires and their contribution to regional haze episodes. *International Journal of Wildland Fire* **27**, 293–312. doi:10.1071/WF17084.

Huang X, Gao J (2021) A review of near-limit opposed fire spread. *Fire Safety Journal* **120**, 103141. doi:10.1016/j.firesaf.2020.103141.

Huang X, Rein G (2016) Interactions of Earth's atmospheric oxygen and fuel moisture in smouldering wildfires. *Science of the Total Environment* **572**, 1440–1446. doi:10.1016/j.scitotenv.2016.02.201.

Huang X, Rein G (2017) Downward spread of smouldering peat fire: The role of moisture, density and oxygen supply. *International Journal of Wildland Fire* **26**, 907–918. doi:10.1071/WF16198.

Huang X, Rein G (2019) Upward-and-downward spread of smoldering peat fire. *Proceedings of the Combustion Institute* **37**, 4025–4033. doi:10.1016/j.proci.2018.05.125.

Huang X, Restuccia F, Gramola M, Rein G (2016) Experimental study of the formation and collapse of an overhang in the lateral spread of smouldering peat fires. *Combustion and Flame* **168**, 393–402. doi:10.1016/j.combustflame.2016.01.017.

Iinuma Y, Brüggemann E, Gnauk T, Müller K, Andreae MO, Helas G, Parmar R, Herrmann H (2007) Source characterization of biomass burning particles: The combustion of selected European conifers, African hardwood, savanna grass, and German and Indonesian peat. *Journal of Geophysical Research Atmospheres* **112**,. doi:10.1029/2006JD007120.

Jones RE, Winters HF, Maissel LI (1968) Effect of Oxygen on the rf-Sputtering Rate of SiO2. *Journal of Vacuum Science and Technology* **5**, 84–87. doi:10.1116/1.1492586.

Kinsman L, Torero JL, Gerhard JI (2017) Organic liquid mobility induced by smoldering remediation. *Journal of Hazardous Materials* **325**, 101–112. doi:10.1016/j.jhazmat.2016.11.049.

Law CK (2010) 'Combustion Physics.' (Cambridge university press)

Lin S, Cheung YK, Xiao Y, Huang X (2020) Can rain suppress smoldering peat fire? *Science of the Total Environment* **727**, 138468. doi:10.1016/j.scitotenv.2020.138468.

Lin S, Chow TH, Huang X (2021) Smoldering propagation and blow-off on consolidated fuel under external airflow. *Combustion and Flame* **234**, 111685. doi:10.1016/j.combustflame.2021.111685.

Lin S, Huang X (2021) Quenching of smoldering: Effect of wall cooling on extinction. *Proceedings of the Combustion Institute* **38**, 5015–5022. doi:10.1016/j.proci.2020.05.017.

Lin S, Huang X, Gao J, Ji J (2021) Extinction of Wood Fire: A Near-Limit Blue Flame Above Hot Smoldering Surface. *Fire Technology*. doi:10.1007/s10694-021-01146-6.

Lin S, Sun P, Huang X (2019) Can peat soil support a flaming wildfire? *International Journal of Wildland Fire* **28**, 601–613. doi:10.1071/WF19018.

Martins MF, Salvador S, Thovert J-F, Debenest G (2010) Co-current combustion of oil shale–Part 1: Characterization of the solid and gaseous products. *Fuel* **89**, 144–151.

Melody SM, Johnston FH (2015) Coal mine fires and human health: What do we know? *International Journal of Coal Geology* **152**, 1–14.

Michel C, Liousse C, Grégoire J, Tansey K, Carmichael GR, Woo J (2005) Biomass burning emission inventory from burnt area data given by the SPOT-VEGETATION system in the frame of TRACE-P and ACE-Asia campaigns. *Journal of Geophysical Research: Atmospheres* **110**,.

Ohlemiller TJTJ (1985) Modeling of smoldering combustion propagation. *Progress in Energy and Combustion Science* **11**, 277–310. doi:10.1016/0360-1285(85)90004-8.

Palmer KN (1957) Smouldering combustion in dusts and fibrous materials. *Combustion and Flame* **1**, 129–154. doi:10.1016/0010-2180(57)90041-X.

Pironi P, Switzer C, Rein G, Fuentes A, Gerhard JI, Torero JL (2009) Small-scale forward smouldering experiments for remediation of coal tar in inert media. *Proceedings of the Combustion Institute* **32**, 1957–1964. doi:10.1016/j.proci.2008.06.184.

Quintiere JG (2006) 'Fundamental of Fire Phenomena.' (John Wiley: New York) doi:10.1002/0470091150.

Rashwan TL, Gerhard JI, Grant GP (2016) Application of self-sustaining smouldering combustion for the destruction of wastewater biosolids. *Waste Management* **50**, 201–212. doi:10.1016/j.wasman.2016.01.037.

Rein G (2009) Smouldering Combustion Phenomena in Science and Technology. *International Review of Chemical Engineering* **1**, 3–18. http://www.era.lib.ed.ac.uk/handle/1842/1152.

Rein G (2013) Smouldering Fires and Natural Fuels. 'Fire Phenom. Earth Syst.' (Ed Claire M. Belcher) pp. 15–34. (John Wiley & Sons, Ltd.: New York) doi:10.1002/9781118529539.ch2.

Rein G (2014) Smoldering Combustion. *SFPE Handbook of Fire Protection Engineering* **2014**, 581–603. doi:10.1007/978-1-4939-2565-0_19.

Rein G, Cohen S, Simeoni A (2009) Carbon emissions from smouldering peat in shallow and strong fronts. *Proceedings of the Combustion Institute* **32**, 2489–2496. doi:10.1016/j.proci.2008.07.008.

Rich D, Lautenberger C, Torero JL, Quintiere JG, Fernandez-Pello C (2007) Mass flux of combustible solids at piloted ignition. *Proceedings of the Combustion Institute* **31 II**, 2653–2660. doi:10.1016/j.proci.2006.08.055.

Santoso MA, Christensen EG, Yang J, Rein G (2019) Review of the Transition From Smouldering to Flaming Combustion in Wildfires. *Frontiers in Mechanical Engineering* **5**,.

doi:10.3389/fmech.2019.00049.

Shin D, Choi S, C. S, S. C (2000) The combustion of simulated waste particles in a fixed bed. *Combustion and Flame* **121**, 167–180. doi:10.1016/S0010-2180(99)00124-8.

Song Z, He T, Li M, Wu D, You F (2022) Self-sustaining smoldering as a novel disposal approach for food waste with high moisture content. *Fuel Processing Technology* **228**, 107144. doi:10.1016/j.fuproc.2021.107144.

Tarelho LAC, Neves DSF, Matos MAA (2011) Forest biomass waste combustion in a pilot-scale bubbling fluidised bed combustor. *Biomass and Bioenergy* **35**, 1511–1523. doi:10.1016/j.biombioe.2010.12.052.

Tillman DA (2000) Biomass cofiring: The technology, the experience, the combustion consequences. *Biomass and Bioenergy* **19**, 365–384. doi:10.1016/S0961-9534(00)00049-0.

Tissari J, Lyyränen J, Hytönen K, Sippula O, Tapper U, Frey A, Saarnio K, Pennanen AS, Hillamo R, Salonen RO, Hirvonen MR, Jokiniemi J (2008) Fine particle and gaseous emissions from normal and smouldering wood combustion in a conventional masonry heater. *Atmospheric Environment* **42**, 7862–7873. doi:10.1016/j.atmosenv.2008.07.019.

Torero JL, Gerhard JI, Martins MF, Zanoni MAB, Rashwan TL, Brown JK (2020) Processes defining smouldering combustion: Integrated review and synthesis. *Prog. Energy Combust. Sci.* **81**, 100869. doi:10.1016/j.pecs.2020.100869.

Vantelon J-P, Lodeho B, Pignoux S, Ellzey JL, Torero JL (2005) Experimental observations on the thermal degradation of a porous bed of tires. *Proceedings of the Combustion Institute* **30**, 2239–2246. doi:https://doi.org/10.1016/j.proci.2004.08.109.

Wang H, van Eyk PJ, Medwell PR, Birzer CH, Tian ZF, Possell M (2017) Effects of Oxygen Concentration on Radiation-Aided and Self-sustained Smoldering Combustion of Radiata Pine. *Energy & Fuels* **31**, 8619–8630. doi:10.1021/acs.energyfuels.7b00646.

Wang H, van Eyk PJ, Medwell PR, Birzer CH, Tian ZF, Possell M, Huang X (2021) Smouldering fire and emission characteristics of Eucalyptus litter fuel. *Fire and Materials* 1–11. doi:10.1002/fam.3004.

Van Der Werf GR, Randerson JT, Giglio L, Collatz GJ, Kasibhatla PS, Arellano Jr AF (2006) Interannual variability of global biomass burning emissions from 1997 to 2004.

Wiedinmyer C, Quayle B, Geron C, Belote A, McKenzie D, Zhang X, O'Neill S, Wynne KK (2006) Estimating emissions from fires in North America for air quality modeling. *Atmospheric Environment* **40**, 3419–3432.

Yerman L, Cormier D, Fabris I, Carrascal J, Torero JL, Gerhard JI, Cheng YL (2017) Potential Bio-oil Production from Smouldering Combustion of Faeces. *Waste and Biomass Valorization* **8**, 329–338. doi:10.1007/s12649-016-9586-1.

Yermán L, Hadden RM, Carrascal J, Fabris I, Cormier D, Torero JL, Gerhard JI, Krajcovic M, Pironi P, Cheng Y-L (2015) Smouldering combustion as a treatment technology for faeces : exploring the parameter space. *Fuel* **147**, 108–116. doi:10.1016/j.fuel.2015.01.055.

Yermán L, Wall H, Torero JL (2017) Experimental investigation on the destruction rates of organic waste

with high moisture content by means of self-sustained smoldering combustion. *Proceedings of the Combustion Institute* **36**, 4419–4426. doi:10.1016/j.proci.2016.07.052.

Zanoni MAB, Torero JL, Gerhard JI (2019) The role of local thermal non-equilibrium in modelling smouldering combustion of organic liquids. *Proceedings of the Combustion Institute* **37**, 3109–3117. doi:10.1016/j.proci.2018.05.177.

Appendix

The wood chips sample was pulverized into powders and dried at 90 °C for 48 h. The thermogravimetric analysis (TGA) was conducted with a PerkinElmer STA 6000 Simultaneous Thermal Analyzer. The initial mass was about 3 mg, and samples were heated at the constant rates of 30 K/min. Two oxygen concentrations were selected, 0% (nitrogen) and 21% (air), with a flow rate of 50 mL/min. Experiments were repeated twice for each case, and good repeatability is shown.

Fig. A1 shows the (a) mass fraction and (b) mass loss rate curves of this wood chips. From the mass-fraction (TG) curves (Fig. A1a), it can be observed that the pyrolysis could consume nearly 70% of the wood fuel. Regardless of the oxygen concentration, the mass loss rate rapidly increases at about 250 °C, which can be defined as the pyrolysis temperature.

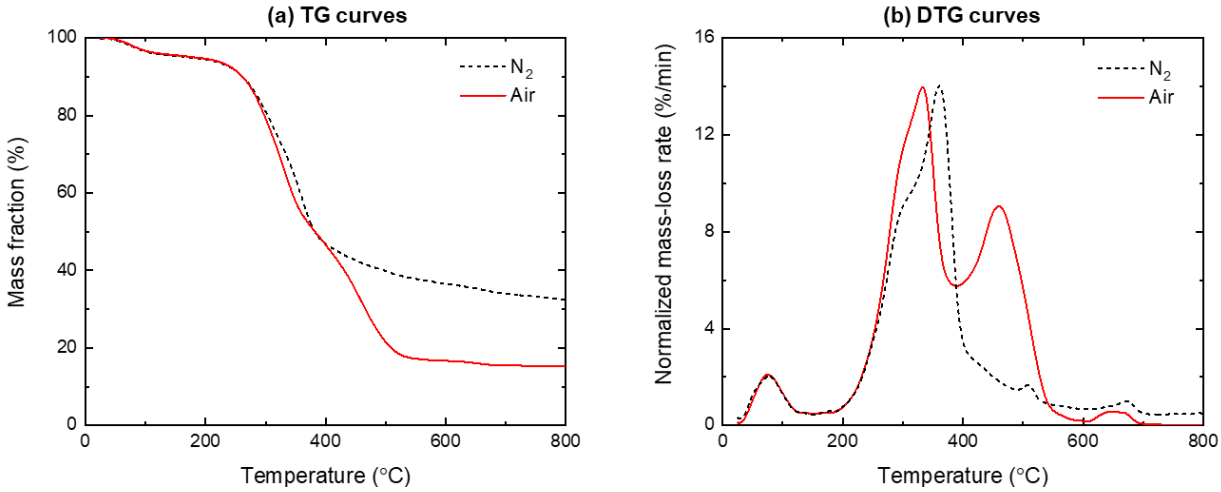

Fig. A1. TGA results of the wood chips at a heating rate of 30 K/min.